EMI R&D PROJECT FINAL REPORT

All the following mandatory information needs to be provided.

Project Title:	Gravity Waves and Turbulence in the Free Atmosphere and the Atmospheric Boundary Layer
Computer Project Account:	spdescan
Start Year - End Year :	2024 - 2026
Principal Investigator(s)	Dr. Andreas Dörnbrack
Affiliation/Address:	DLR Oberpfaffenhofen Institut für Physik der Atmosphäre Münchener Str. 20 **D – 82230 WESSLING** Germany
Other Researchers (Name/Affiliation):	Dr. Sonja Gisinger Dr. Andreas Schäfler Dr. Antonia Englberger Michael Binder

Summary of project objectives

(10 lines max)

This special project aims at combining high-resolution ground-based and airborne observations with IFS operational forecasts and analyses, with reanalyses, and with results from numerical modelling. The base of our measurements are airborne in-situ observations of the atmospheric wind and temperature in the upper troposphere and lower stratosphere as well as ground-based and airborne remote-sensing observations of temperature in the middle atmosphere. The goal is to analyse the properties of internal gravity waves and of turbulence in the stably stratified atmospheric airflow. A new aspect of our research will be the numerical simulation of the stably stratified atmospheric boundary layer where similar turbulent bursts are observed as in the free atmosphere. The challenge for numerical modelling is to achieve the needed high spatial and temporal resolutions. Furthermore, in this project we want to address the transition to modern computer architectures by applying the newly developed FVM of ECMWF to selected problems.

Summary of problems encountered

No problems arose. We appreciate the trustworthy, reliable, and fast access to the ECMWF's IFS forecast and analysis data. This type of access has facilitated—and indeed made possible—both the planning of a wide variety of aircraft measurement campaigns and their evaluation. As part of this project, we have established our own infrastructure at the DLR Institute of Atmospheric Physics, which enables participants in the measurement campaigns to use specific and customized visualizations of the IFS products, see for example Binder et al. (2026).

The computing resources were used primarily to access IFS products via the HPC facilities. The originally planned trial of HPC for boundary layer research was not carried out at the ECMWF, as additional resources were utilized from German supercomputer centres.

Experience with the EMI R&D Project framework

Communication with "User Support" regarding the special project went very well. For the most part, we received quick, unbureaucratic assistance whenever we encountered technical problems.

Summary of results

The following sections present a selection of the results of this special project, which were achieved through extensive use of ECMWF resources. Sections (1) and (2) are examples of research on internal gravity waves in the middle atmosphere. Additional references in which members of this project are either authors or co-authors include Achatz et al. (2024), Dörnbrack (2024), Dörnbrack et al. (2025), Gupta et al. (2024), Kaifler et al. (2025), and Wing et al. (2025). Section (3) is an excellent example of how the IFS's recently implemented operational CAT index (Bechtold et al., 2021, Dörnbrack et al. 2022) can be used to analyse an occurrence of severe turbulence, particularly by utilizing information from the ensemble forecast system. Currently, we are working to use other aircraft field campaign data to analyse the turbulence in the upper troposphere and lower stratosphere, e.g. Amor et al. (2026) and Dörnbrack et al. (2026). Finally, Section (4) provides a clear example of how observations from field experiments can be used to validate and improve IFS forecasts. Other examples of validation studies of this kind in which members of this project have contributed include Schäfler et al. (2024) and Quinting et al. (2026).

This final report does not mention the numerous publications in the field of contrail research (Dischl et al. 2024, 2025, Harlaß et al. 2024, Märkl et al. 2024, and Voigt et al. 2026). For these publications, the principal investigator (PI) of this project made numerous predictions of ice-saturated regions using the operational IFS high-resolution forecasts. Even though they are hardly mentioned in these publications, these predictions are an indispensable component of the successful measurement flights.

(1) Observing Gravity Waves Generated by Moving Sources with Ground-Based Rayleigh Lidars (Binder and Dörnbrack, 2024)

Temperature measurements by zenith-pointing ground-based Rayleigh lidars are often used to detect middle atmospheric gravity waves, see as examples the plots in Figures 2 and 5. In time-height diagrams of observed or modelled temperature perturbations, stationary mountain waves are identifiable by horizontal phase lines. Vertically tilted phase lines, on the other hand, indicate that the wave source or the propagation conditions are transient. Idealized numerical simulations illustrate that and how a wave source moving in the direction of the mean wind entails upward-tilted phase lines, see Figure 1. The inclination angle depends on the horizontal wavelength and the propagation speed of the wave source.

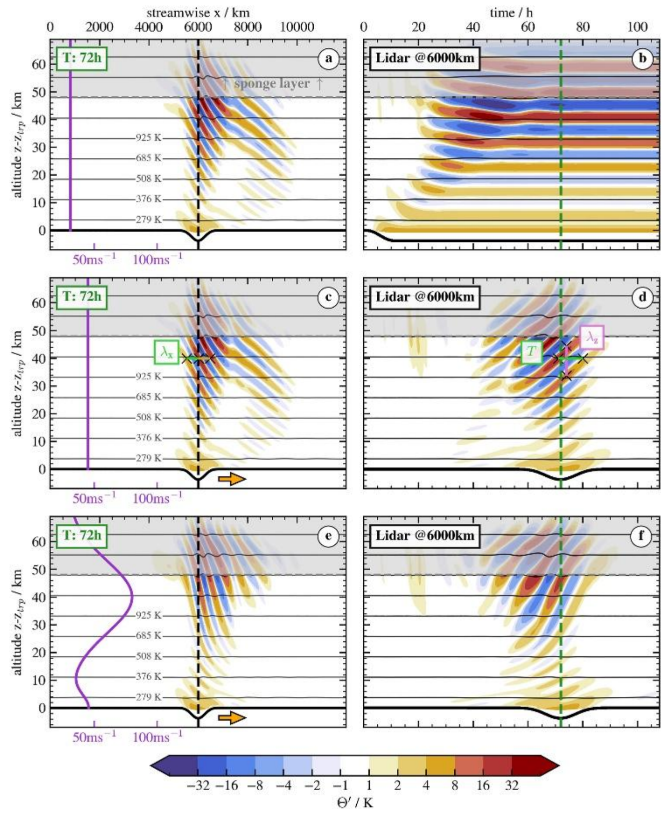

Figure 1: Vertical cross-sections (a), (c) and (e) after t = 72 h with ambient wind profiles in purple and time-height diagrams (b), (d) and (f) at the outlined position for three different simulations. The first simulation (a) and (b) features a stationary obstacle at the lower boundary and a constant wind profile. In the second simulation (c) and (d) the trough moves to the right with a constant speed c_{tf} = 13.88 m s^{-1} and the wind is increased by the same amount. The last simulation (e) and (f) represents a simulation with a more realistic stratospheric wintertime wind profile. The assessment of λ_z and period T from the time-height diagram is labeled in (d), two consecutive λ_x are labeled in (c). Contour lines represent constant potential temperature and the amplitude of the lower boundary is scaled by a factor of 5.

On this basis, the goal of the study was to identify and characterize non-orographic gravity waves (NOGWs) from propagating sources, for example, upper-level jet/front systems, in simulated lidar observations and actual Rayleigh lidar measurements, see Figure 2. Composites of selected atmospheric variables from meteorological forecasts or reanalysis data are thoughtfully combined to associate NOGWs with processes in the troposphere and stratosphere, see Figure 3.

The example also emphasizes that temporal filtering of temperature measurements is appropriate for NOGWs, especially in the presence of a strong polar night jet that implies large vertical wavelengths. During two selected observational periods of the COmpact Rayleigh Autonomous Lidar (CORAL) in the lee of the southern Andes, upward-tilted phase lines are mainly associated with mountain waves and transient background wind conditions. One night-time measurement by CORAL coincides with the passage of an upper-level trough, but large-amplitude mountain waves superpose the small-amplitude NOGWs in the middle atmosphere.

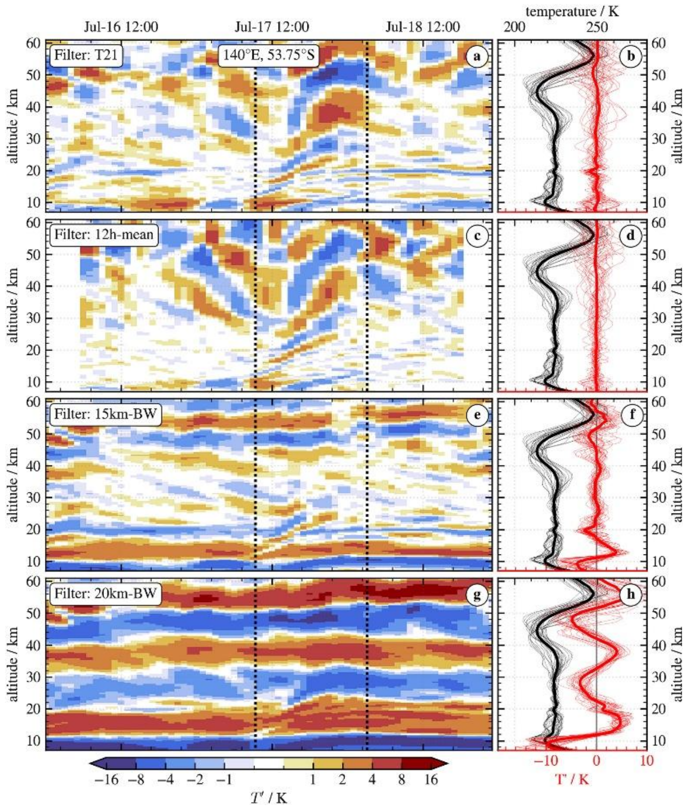

Figure 2: Time-height diagrams of stratospheric ERA5 T' for a location (140°E, 53.75°S) over the Southern Ocean (left column) and corresponding vertical profiles of absolute temperature and temperature perturbations (right column). Thick black and red lines in (b), (d), (f) and (h) are temporal mean profiles of absolute temperature and T', respectively. Thin lines are individual profiles every 2 h. Panels (a) and (b) show temperature perturbations after subtracting the truncated temperature field T21 (horizontally filtered by removing wave numbers larger than 21) of the ERA5 dataset. Panels (c) and (d) show T' after removing a temporal running mean of 12 h Panels (e) and (f) display the result of a vertical high pass Butterworth filter with a cutoff wavelength λ_{cut} = 15 km and panels (g) and (h) with λ_{cut} = 20 km.

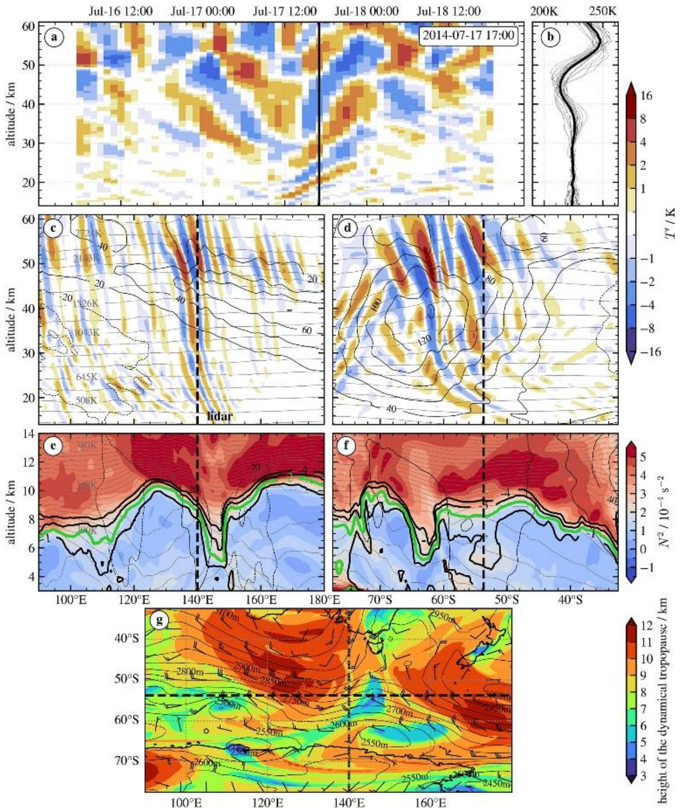

Figure 3: ERA5 overview for a location over the Southern Ocean (53.75°S, 140°E) during research flight RF25 of the DEEPWAVE campaign. Panels (a) and (b) are similar to Figures 2(c) and 2(d) emulating the measurements of a vertically staring ground-based lidar. Panels (c) and (d) are vertical sections of stratospheric T' along sectors of the latitude circle (c) and meridian (d) of the virtual lidar location. (e) and (f) are corresponding vertical sections of thermal stability N^2 (10^{-4} s^{-2}, color-coded), potential temperature (K, thin gray lines), and potential vorticity (1, 2, 4 PVU: black, 2 PVU: green) in the vicinity of the dynamical tropopause. Thin black lines in the vertical sections are zonal (d) and (f) and meridional (c) and (e) wind components (solid: positive, dashed: negative). Panel (g) is a horizontal section of the height of the 2 PVU surface (km, color-coded), geopotential height (m, solid lines) and wind barbs at the 850 hPa level. The black vertical line in (a) marks the time (17 July 2014, 17 UTC) for (c)–(g) and dashed lines in (c)–(g) highlight the location of the virtual lidar and profiles in (a) and (b).

(2) Estimates of Southern Hemispheric Gravity Wave Momentum Fluxes across Observations, Reanalyses, and Kilometer-Scale Numerical Weather Prediction Model (Gupta et al., 2024)

Gravity waves are among the key drivers of the meridional overturning circulation in the mesosphere and upper stratosphere. Their representation in general circulation models suffers from insufficient resolution and limited observational constraints on their parameterizations. Both restrictions obscure assessments of middle atmospheric circulation changes in a changing climate. The study by Gupta et al. (2024) presents for a first time a comprehensive analysis of stratospheric gravity wave activity in an area above and downstream of the Andes from 1 to 15 August 2019, see Figure 4. Here, the special focus is on the representation of gravity waves ranging from an unprecedented kilometer-scale global forecast model (1.4 km ECMWF IFS, see Polichtchouk et al. 2023[1]), ground-based Rayleigh lidar (CORAL) observations at Rio Grande, Argentina[2], modern reanalysis (ERA5), to a coarse-resolution climate model (EMAC), see Figures 5 and 6.

[1] Polichtchouk, I., A. van Niekerk, and N. Wedi, 2023: Resolved gravity waves in the extratropical stratosphere: Effect of horizontal resolution increase from $O(10)$ to $O(1)$ km. *J. Atmos. Sci.*, **80**, 473–486, https://doi.org/10.1175/JAS-D-22-0138.1.

[2] Kaifler, N., B. Kaifler, A. Dörnbrack, M. Rapp, J. L. Hormaechea, and A. de la Torre, 2020: Lidar observations of large-amplitude mountain waves in the stratosphere above Tierra del Fuego, Argentina. *Sci. Rep.*, **10**, 14529, https://doi.org/10.1038/s41598-020-71443-7.

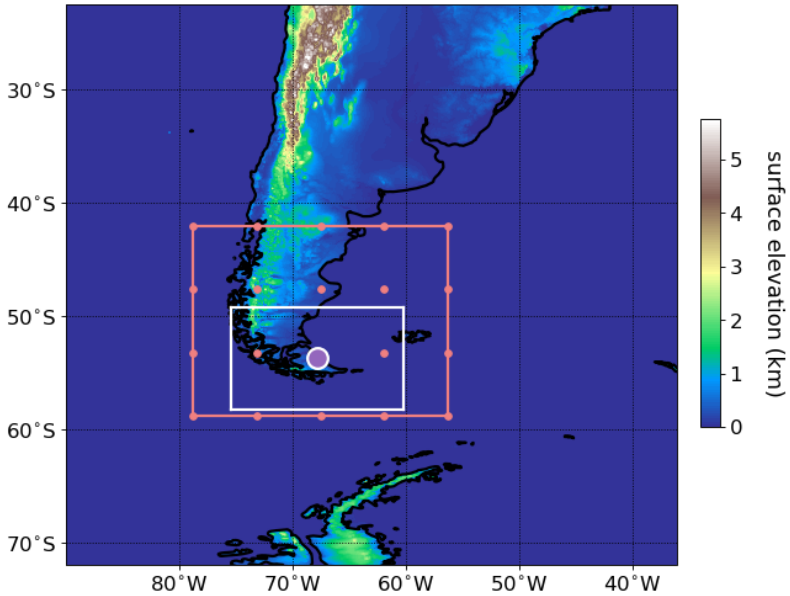

Figure 4: Variations in surface topography are shown in color using cylindrical projection. The violet dot shows the location of CORAL lidar at Rio Grande. The white box shows the 1000 km × 1000 km box around Rio Grande used for two-dimensional wavelet analysis. The red grid box and dots shows the T21 grid used to conservatively interpolate high-resolution fluxes from IFS-1km and ERA5.

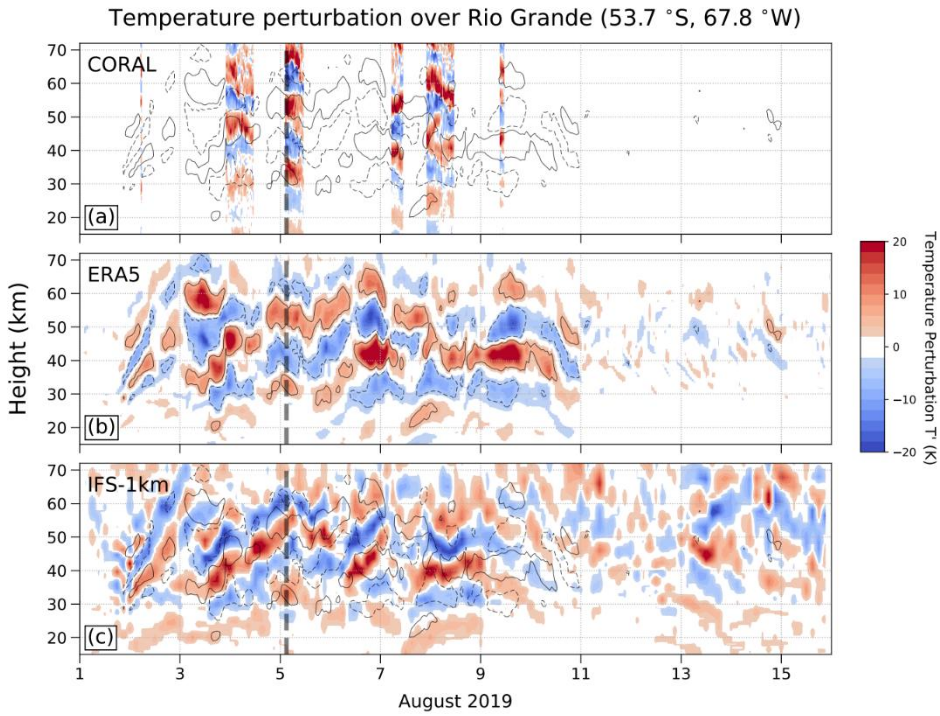

Figure 5: Vertical profiles of gravity wave-induced temperature perturbations (color) during 1-15 August 2019 over Rio Grande, Argentina (53.7 °S, 67.8 °W) from (a) ground-based Rayleigh lidar CORAL, (b) ERA5 reanalysis, and (c) ECMWF's IFS-1km free running model. The black curves in a-c show the ± 5 K temperature anomaly contours from ERA5, and are overlaid for reference. The dashed vertical bars in a-c mark the time 5 August 2019 03 UTC for which the horizontal profile of the GWs for ERA5 and IFS-1km are shown in Figure 6.

Resolved vertical flux of zonal gravity wave momentum (GWMF) is found to be stronger by a factor of at least 2–2.5 in IFS compared to ERA5. Compared to resolved GWMF in IFS, parameterizations in ERA5 and EMAC continue to inaccurately generate excessive GWMF poleward of 60°S, yielding prominent differences between resolved and parameterized GWMFs. A like-to-like validation of GW profiles in IFS and ERA5 reveals similar wave structures. Still, even at ~1 km resolution, the resolved waves in IFS are weaker than those observed by lidar.

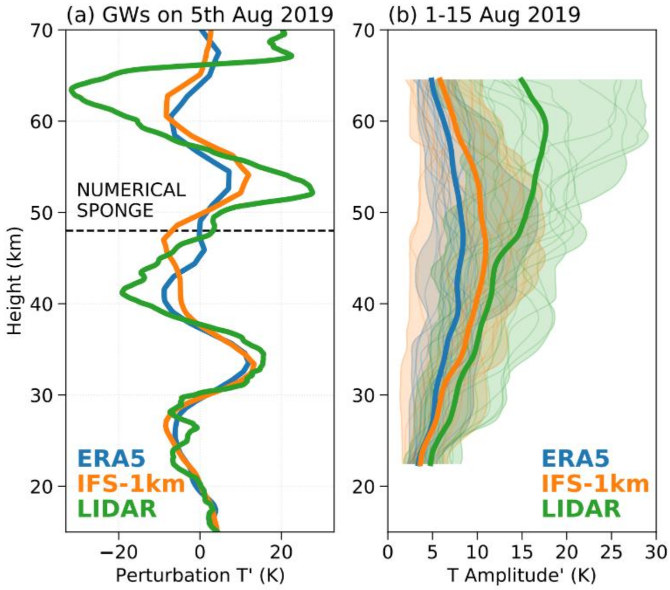

Figure 6: (a) Vertical profiles of temperature perturbations over Rio Grande in CORAL (green), IFS (orange), and ERA5 (blue), on 5 August 2019 03 UTC. The dashed black horizontal bar at 48 km marks the introduction of the mesospheric sponge. (b) Gravity wave amplitudes in the three models, obtained by vertically averaging the temperature magnitude over a centred 15-km vertical window. The bold curves show the time mean amplitude, while the individual thin curves enclosed within the respective shaded regions show the amplitudes at all the individual snapshots during 1-15 August 2019 for which the data is available.

Further, estimates of the gravity wave momentum fluxes across the datasets reveal that temperature-based proxies, based on mid-frequency approximations for linear gravity waves, overestimate its magnitude due to simplifications and uncertainties in estimates of the horizontal wavelength from data. Overall, the analysis provides GWMF benchmarks for parameterization validation and calls for three-dimensional gravity wave parameterizations, better upper-boundary treatment, and vertical resolution increases commensurate with increases in horizontal resolution in models, for a more realistic gravity wave analysis.

(3) Severe Convectively Induced Turbulence Hitting a Passenger Aircraft and Its Forecast by the ECMWF IFS Model (Gisinger et al. 2024)

Atmospheric turbulence poses a major risk to aviation. Besides airframe damage, it can cause injuries of passengers and crew when encountered unexpectedly. The Singapore Airlines flight SQ321 was on its way from London to Singapore when severe turbulence was encountered over Myanmar on 21 May 2024, see Figure 7. This study analysed how well the turbulence was predicted by the computed turbulent eddy dissipation rate (EDR) forecast index of the ECMWF IFS. It was found that ECMWF IFS was able to predict the convection and associated turbulence 24 h in advance. The state-of-the-art probabilistic EDR forecasts based on IFS ensemble members predicted probabilities for EDR > 0.18 $m^{2/3}$ s^{-1} between 10% and 40% over Myanmar with higher values for shorter lead time (8 h forecast). Individual members predicted EDR > 0.18 $m^{2/3}$ s^{-1}. Knowledge about the characteristics of convection in the IFS forecasts is required to make proper use of the probabilities determined from the ensemble for such cases.

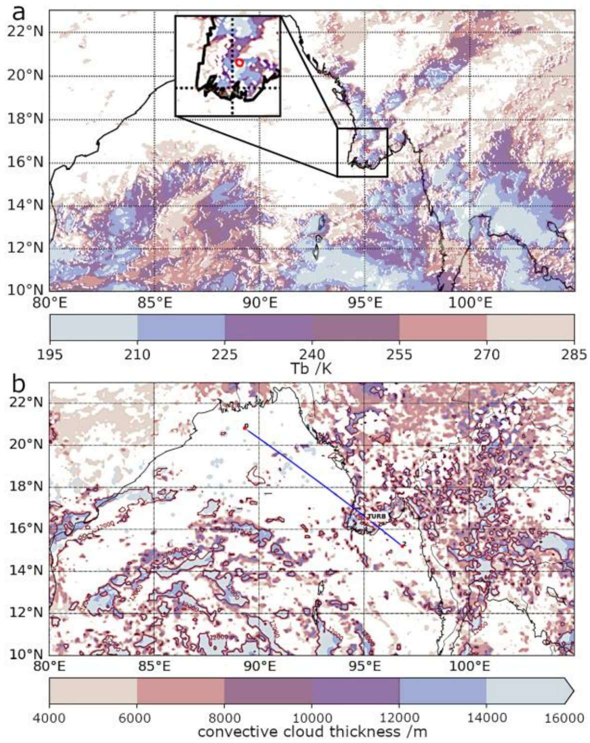

Figure 7: (a) Satellite image of Himawari-8 showing the developing convective clouds by means of brightness temperature (Tb) on 21 May 2024 08 UTC. The red circle shown at location TURB has a diameter of approximately 10 km. The insert shows a zoom to the region of the incident. (b) ECMWF IFS forecast showing the thickness of convective clouds (= height of convective cloud top by parameterized convection minus cloud base height) on 21 May 2024 08 UTC visualized with the MSS tool[3]. Heights of the convective cloud top of 12000 m are marked by the dark red isolines. The forecast was initialized on 20 May 2024 00 UTC.

Every day, the IFS forecasts—initialized at 00 UTC—become available around 09 UTC on the same day, following their calculation. Figure 8 shows the 12 h time series of the IFS EDR forecast at 240 hPa at the location of the turbulence encounter (TURB) of flight SQ321, which departed from London on 20 May 2024 at 21:38 UTC. The IFS forecast, which was initialized on May 20, 2024, at 00 UTC, is the most recent forecast available prior to departure; therefore, the airline could have used it to warn the crew and passengers. This HRES forecast shows a maximum in EDR of 0.30 $m^{2/3}$ s^{-1} at 07 UTC followed by low values less than 0.1 $m^{2/3}$ s^{-1} afterward until 12 UTC which is 21:30 local time in Myanmar. These HRES values lie at the upper edge when compared to the other 50 IFS ENS ensemble members at 06 UTC and 07 UTC and close to the median at 08 UTC. The IFS ENS shows an increase of the 90th percentile from about 0.12 $m^{2/3}$ s^{-1} at 06 UTC to about 0.2 $m^{2/3}$ s^{-1} at 08 UTC while the median remains well below 0.1 $m^{2/3}$ s^{-1}.

The HRES forecast initialized a day later on 21 May 00 UTC shows a maximum in EDR of 0.2 $m^{2/3}$ s^{-1} at 08 UTC which is close to the 90th percentile of the ENS. However, individual members show values well above 0.2 $m^{2/3}$ s^{-1} at 07 UTC and 08 UTC just in between the time when the turbulence encounter of flight SQ321 happened at 07:49 UTC. Additional sensitivity runs with the IFS ENS show a narrow distribution with EDR close to 0.05 $m^{2/3}$ s^{-1} when only contributions by the vertical diffusion scheme are considered and the terms for convection are omitted (Bechtold et al., 2021).

[3] Rautenhaus, M., Bauer, G., & Dörnbrack, A. (2012). A web service based tool to plan atmospheric research flights. *Geoscientific Model Development*, 5(1), 55–71. https://doi.org/10.5194/gmd-5-55-2012

The probability for EDR > 0.18 $m^{2/3}$ s^{-1} determined from the ENS members of the forecast initialized on 20 May 2024 00 UTC is 12% for 08 UTC at 240 hPa at TURB. When the ENS EDR maxima of ± 2 grid points from TURB (± 0.2° in latitude and longitude, respectively) are considered, which incorporates the uncertainty of the location of convection among the ENS members, the probability for EDR increases to 36%. Horizontal maps of EDR at 240 hPa for both HRES forecasts are shown for the time of maximum EDR at TURB, that is 07 UTC for initialization on 20 May 00 UTC (Figure 8b) and 08 UTC for the initialization on 21 May 00 UTC (Figure 8c). Enhanced EDR is mainly found over land and in the ITCZ which corresponds to the occurrence of convection.

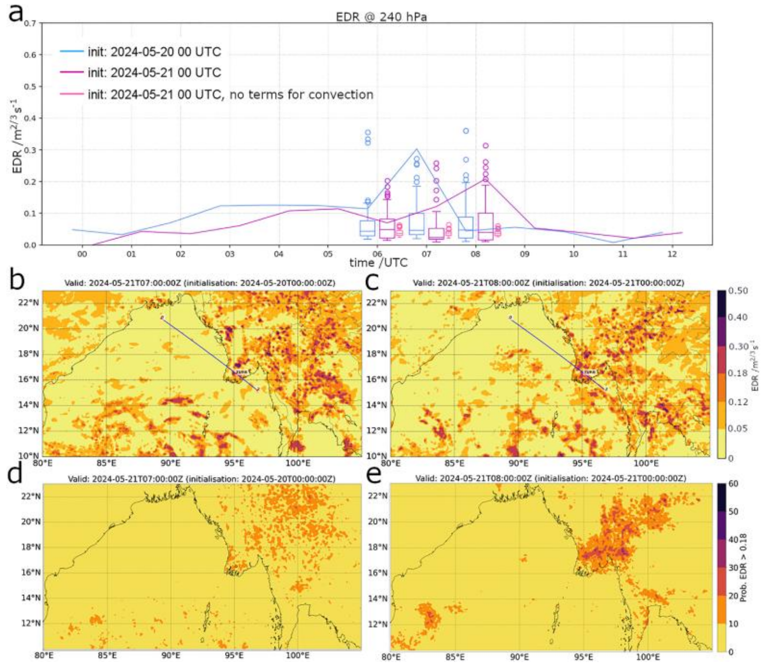

Figure 8: (a) Time series showing EDR at 240 hPa at the location of the incident (TURB) for the IFS HRES forecasts initialized on 20 May 2024 00 UTC with lead time 24–36 h (blue) and initialized on 21 May 2024 00 UTC with lead time 0–12 h (purple). Boxplot shows the corresponding IFS ENS (median, 10th/90th percentiles, and maximum extremes) for 06, 07, and 08 UTC including (blue, purple) and without terms for convection (pink) in computing the EDR in the IFS turbulence predictors. (b) EDR ($m^{2/3}$ s^{-1}) at 240 hPa on 21 May 2024 07 UTC of the ECMWF IFS HRES forecast initialized on 20 May 2024 00 UTC (lead time 31 hr) and (c) on 21 May 2024 08 UTC of the ECMWF IFS HRES forecast initialized on 21 May 2024 00 UTC (lead time 8 h). Maps were visualized with the MSS tool (d), (e) Corresponding probability for EDR > 0.18 $m^{2/3}$ s^{-1} computed from the IFS ENS.

It is the convective momentum transport that dominated the IFS EDR forecast that day. Both HRES forecasts agree as such that they show the highest risk to encounter severe turbulence along the flight track over Myanmar (Figures 8b and 8c) near the location of the turbulence encounter of flight SQ321. Horizontal maps of the ENS probability for EDR > 0.18 $m^{2/3}$ s^{-1} (Figures 8d and 8e) reveal probabilities of 10%–20% over land associated with the predicted occurrence of convection. Local probabilities of 30%–40% were found for shorter lead time (initialized on 21 May 2024 00 UTC, lead time 8 h) and the area with enhanced probabilities becomes more focused in a band-like pattern (Figure 8e) which compares well with the convection in the satellite image (Figure 7a).

The results presented in this study show that the turbulence forecasts available from ECMWF provide valuable information on convection and convectively induced turbulence, as encountered by flight SQ321, along route prior to departure. As such the IFS forecast could have helped to make the crew aware of potential occurrence of turbulence by convection in the area and to take precautions like switching on the fasten seat belt sign, postponing board service, and request updates by nowcasting services. The implementation of a probabilistic turbulence forecast based on the IFS ensemble was essential. However, training is required in order to learn the characteristics of the IFS forecasts for convection and to make proper use of the ENS probabilities for moderate and severe turbulence.

(4) Influence of radiosonde observations on the sharpness and altitude of the midlatitude tropopause in the ECMWF IFS (Krüger et al. 2024)

Initial conditions of current numerical weather prediction systems insufficiently represent the sharp vertical gradients across the midlatitude tropopause. Data assimilation may provide a means to improve tropopause structure by correcting the erroneous background forecast towards the observations. In this study, the influence of assimilating radiosonde observations on tropopause structure, i.e., the sharpness and altitude, is investigated in the ECMWF's IFS. Altogether, 9729 midlatitude radiosondes launched during 1 month in autumn 2016 are evaluated. About 500 of these radiosondes, launched on request during the North Atlantic Waveguide Downstream Impact Experiment (NAWDEX) field campaign, are used to set up an observing system experiment (OSE) that comprises two assimilation forecast experiments, one run with and one without the non-operational soundings (Figure 9).

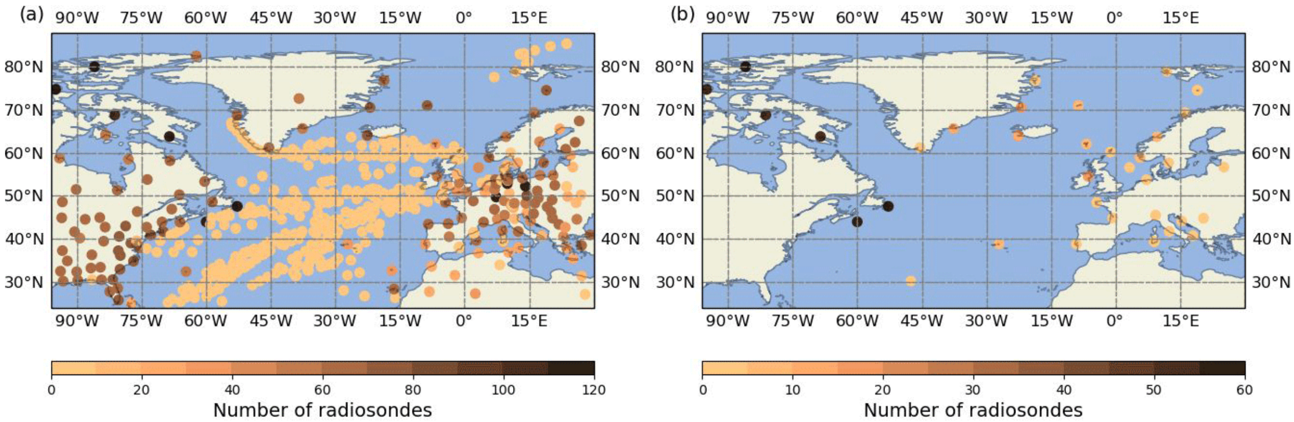

Figure 9. Positions of radiosonde launches that were assimilated by the ECMWF IFS between 17 September and 18 October 2016 for **(a)** all radiosondes (9729) and **(b)** the subset of 497 non-operational radiosondes launched during NAWDEX. The coloring denotes the number of assimilated profiles at a particular site. The scale of the color bar changes between **(a)** and **(b)**.

The influence on the tropopause is assessed in a statistical, tropopause-relative evaluation of observation departures of temperature, static stability (N^2), wind speed, and wind shear from the background forecast and the analysis (Figure 10). Temperature is overestimated by the background at the tropopause (warm bias, ~ 1 K) and underestimated in the lower stratosphere (cold bias, −0.3 K) leading to an underestimation of the abrupt increase in N^2 at the tropopause.

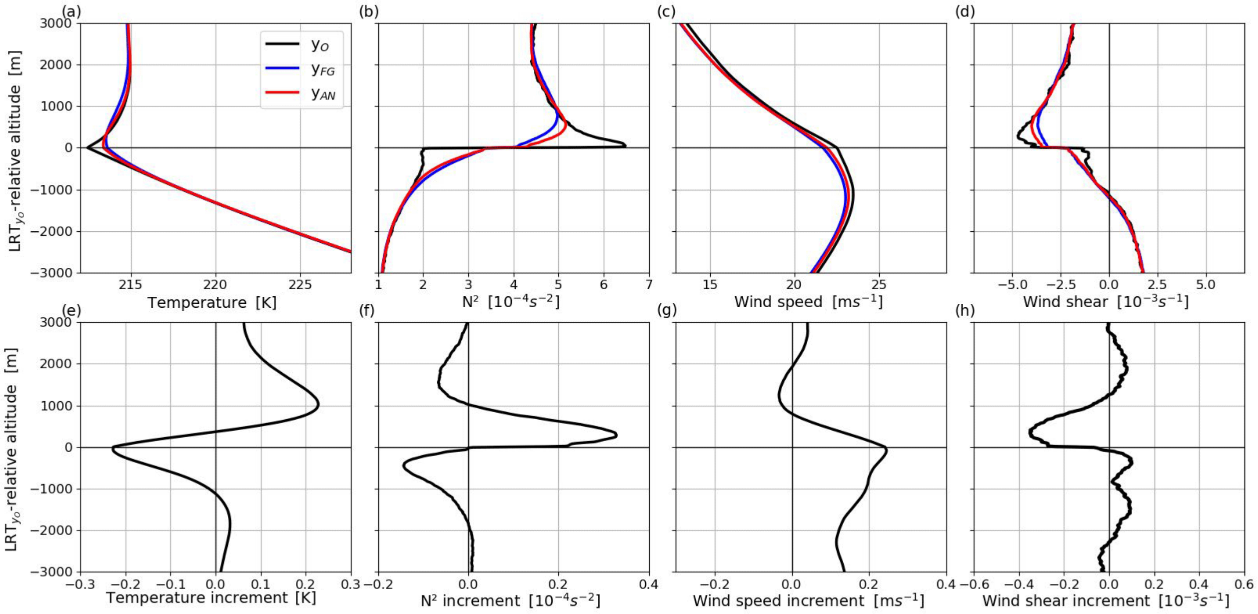

Figure 10. LRT$_{yO}$-relative distributions of **(a)** temperature, **(b)** N^2, **(c)** wind speed, and **(d)** wind shear, as well as the respective increments (**(e–h)**), averaged for the 9729 profiles of observations (black line), background (blue line), and analysis (red line).

The increments (differences in analysis and background) reduce these background biases and improve tropopause sharpness. Profiles with sharper tropopause exhibit stronger background biases but also an increased positive influence of the observations on temperature and N^2 in the analysis. Wind speed is underestimated in the background, especially in the upper troposphere ($\sim 1\,\mathrm{m\,s^{-1}}$), but the assimilation improves the wind profile. For the strongest winds the background bias is roughly halved. The positive influence on the analysis wind profile is associated with an improved vertical distribution of wind shear, particularly in the lower stratosphere.

We furthermore detect a shift in the analysis tropopause altitude towards the observations. The evaluation of the OSE highlights that the diagnosed tropopause sharpening can be primarily attributed to the radiosondes. This study shows that data assimilation improves wind and temperature gradients across the tropopause, but the sharpening is small compared with the model biases. Hence, the analysis still systematically underestimates tropopause sharpness which may negatively impact weather and climate forecasts.

List of publications/reports from the project with complete references

1. Achatz, U., J. M. Alexander, E. Becker, H.-Y. Chun, **A. Dörnbrack**, L. Holt, R. Plougonven, I. Polichtchouk, K. Sato, A. Sheshadri, C. C. Stephan, A. van Niekerk, and C. J. Wright, 2024: Atmospheric Gravity Waves: Processes and Parameterization, *Journal of the Atmospheric Sciences,* **81**, 237–262, https://doi.org/10.1175/JAS-D-23-0210.1

2. Amor, J. I. V., P. Rodriguez Imazio, **A. Dörnbrack**, L. Vidal, and M. Alvarez Imaz, 2026: Convectively-induced turbulence: High-resolution aircraft measurements over central Argentina, *Journal of Geophysical Research: Atmospheres*, under review.

3. Bechtold, P., M. Bramberger, **A. Dörnbrack**, L. Isaksen, and M. Leutbecher, 2021: Experimenting with a clear air turbulence (CAT) index from the IFS. *ECMWF Technical Memorandum* **874**. https://doi.org/10.21957/4l34tqljm

4. **Binder, M**. and **Dörnbrack, A**., 2024: Observing gravity waves generated by moving sources with ground-based Rayleigh lidars. *Journal of Geophysical Research: Atmospheres*, 129, e2023JD040156. https://doi.org/10.1029/2023JD040156

5. **Binder, M**., Kaifler, B., Kaifler N., 2026: Lidar Calendar, https://extern05.pa.op.dlr.de/ma-lidar-calendar/php_calendar/calendar.php?ym=2018-04&idatetime=20180422-2225&nm_state=0&content=filter1D&lidar=coral, last access 8 July 2026

6. Dischl, R., Sauer, D., Voigt, C., Harlaß, T., Sakellariou, F., Märkl, R., Schumann, U., Scheibe, M., Kaufmann, S., Roiger, A., **Dörnbrack, A**., Renard, C., Gauthier, M., Swann, P., Madden, P., Luff, D., Johnson, M., Ahrens, D., Sallinen, R., Schripp, T., Eckel, G., Bauder, U., and Le Clercq, P., 2024: Measurements of particle emissions of an A350-941 burning 100 % sustainable aviation fuels in cruise, *Atmos. Chem. Phys*., **24**, 11255–11273, https://doi.org/10.5194/acp-24-11255-2024.

7. Dischl, R., R. Märkl, D. Sauer, C. Voigt, T. Harlaß, M. Scheibe, V. Hahn, S. Kaufmann, A. Marsing, **A. Dörnbrack**, A. Roiger, F. Yu, M. Gauthier, C. Renard, P. Swann, M. Johnson, D. Ahrens, R. Sallinen, G. Eckel, and P. Le Clercq, 2025: Fuel sulfur content can modulate contrail ice crystal numbers, *Commun Earth Environ* **6**, 902. https://doi.org/10.1038/s43247-025-02951-5

8. Harlaß, T., Dischl, R., Kaufmann, S., Märkl, R., Sauer, D., Scheibe, M., Stock, P., Bräuer, T., **Dörnbrack, A**., Roiger, A., Schlager, H., Schumann, U., Pühl, M., Schripp, T., Grein, T., Bondorf, L., Renard, C., Gauthier, M., Johnson, M., Luff, D., Madden, P., Swann, P., Ahrens, D., Sallinen, R., and Voigt, C., 2024: Measurement report: In-flight and ground-based measurements of nitrogen oxide emissions from latest-generation jet engines and 100 % sustainable aviation fuel, *Atmos. Chem. Phys*., **24**, 11807–11822, https://doi.org/10.5194/acp-24-11807-2024.

9. **Dörnbrack, A**., P. Bechtold, and U. Schumann, 2022: High-resolution aircraft observations of turbulence and waves in the free atmosphere and comparison with global model predictions. *Journal of Geophysical Research: Atmospheres*, **127**, e2022JD036654. https://doi.org/10.1029/2022JD036654

10. **Dörnbrack, A**., 2024: Transient Tropopause Waves, *Journal of the Atmospheric Sciences*, **81**, 1647–1668, https://doi.org/10.1175/JAS-D-24-0037.1

11. **Dörnbrack, A**., Lachnitt, H.-C., Hoor, P., & Imazio, P. R., 2025: Multiscale dynamical processes shaping a mixing line. *Journal of Geophysical Research: Atmospheres*, 130, e2025JD043527. https://doi.org/10.1029/2025JD043527

12. **Dörnbrack, A.**, A. Giez, C. Mallaun, and C. C. Stephan, 2026; Turbulence over the Atlantic ITCZ - Is the upper troposphere above doldrums less turbulent? *Weather and Climate Dynamics*, EGUsphere [preprint], https://doi.org/10.5194/egusphere-2026-2628

13. **Gisinger, S**., Bramberger, M., **Dörnbrack, A.,** and Bechtold, P., 2024: Severe convectively induced turbulence hitting a passenger aircraft and its forecast by the ECMWF IFS model. *Geophysical Research Letters*, **51**, e2024GL113037. https://doi.org/10.1029/2024GL113037

14. Gupta, A., R. Reichert, **A. Dörnbrack**, H. Garny, R. Eichinger, I. Polichtchouk, B. Kaifler, and T. Birner, 2024: Estimates of Southern Hemispheric Gravity Wave Momentum Fluxes across Observations, Reanalyses, and Kilometer-Scale Numerical Weather Prediction Model. *J. Atmos. Sci.*, **81**, 583–604, https://doi.org/10.1175/JAS-D-23-0095.1.

15. Kaifler, B., Kaifler, N., Rapp, M., and **Dörnbrack, A**., 2025: Mountain wave momentum flux estimates from airborne lidar measurements in the middle atmosphere above the Southern Andes. *Journal of Geophysical Research: Atmospheres*, **130**, e2025JD043683. https://doi.org/10.1029/2025JD043683

16. Krüger, K; **Schäfler, A.,** Weissmann, M., and Craig, G. C., 2024: Influence of radiosonde observations on the sharpness and altitude of the midlatitude tropopause in the ECMWF IFS. *Weather Clim. Dynam.,* **5 (2),** 491–509, https://doi.org/10.5194/wcd-5-491-2024.

17. Märkl, R. S., Voigt, C., Sauer, D., Dischl, R. K., Kaufmann, S., Harlaß, T., Hahn, V., Roiger, A., Weiß-Rehm, C., Burkhardt, U., Schumann, U., Marsing, A., Scheibe, M., **Dörnbrack, A**., Renard, C., Gauthier, M., Swann, P., Madden,

P., Luff, D., Sallinen, R., Schripp, T., and Le Clercq, P., 2024: Powering aircraft with 100 % sustainable aviation fuel reduces ice crystals in contrails, *Atmos. Chem. Phys*., **24**, 3813–3837, https://doi.org/10.5194/acp-24-3813-2024

18. Quinting, J., C. M. Grams, B. Kirsch, A. Oertel, A. M. Ramos, S. Raveh-Rubin, and **A. Schäfler**, 2026: Dry Intrusion Connects High-Impact Cyclones Eunice and Franklin: Emerging Observational Targets of NAWDIC. *Bull. Amer. Meteor. Soc.*, **107**, E1302–E1314, https://doi.org/10.1175/BAMS-D-25-0170.1.
19. **Schäfler, A.;** Krüger, K.; Oertel, A.; Quinting, J. F.; Raveh-Rubin, S., 2024: Indication for Biases in Dry Intrusions and the Marine Boundary Layer Over the Azores in ECMWF Short-Term Forecasts and Analyses. *Geophysical Research Letters,* 51, e2024GL109601. https://doi.org/10.1029/2024GL109601.
20. Voigt, C., R. Märkl, D. Sauer, R. Dischl, S. Kaufmann, T. Bräuer, T. Jurkat-Witschas, C. Renard, K. Seeliger, G. Le Chenadec, J. Moreau, E. Requena-Esteban, F. Yu, N. Bonne, M. Vals, A. Roche, J. Zelina, **A. Dörnbrack**, L. Eirenschmalz, C. Heckl, E. Horst, M. Lichtenstern, A. Marsing, G. Neumann, A. Roiger, M. Scheibe; P. Stock, A. Giez, G. Eckel, P. Le Clercq, 2026: Substantial aircraft contrail formation at low soot emission levels. *Nature* **652**, 112–118. https://doi.org/10.1038/s41586-026-10286-0
21. Wing, R., I. Strelnikova, **A. Dörnbrack**, M. Gerding, E. Franco-Diaz, L. Holt, M. Mossad, and G. Baumgarten, 2025: Direct Observation of Quasi-monochromatic Gravity Wave Packets Associated with the Polar Night Jet using a Doppler-Rayleigh lidar. *Journal of Geophysical Research: Atmospheres*, **130**, e2025JD043707. https://doi.org/10.1029/2025JD043707

Future plans

We will continue our work with the EMI R&D Projects by submitting an application for the year 2027-2029 entitled "Forecasting and Validation of Aircraft Field Campaigns".